

Short-Term Behavior of a Geothermal Energy Storage: Modeling and Theoretical Results

Paul Honore Takam · Ralf Wunderlich · Olivier Menoukeu Pamen

Version of April 25, 2023

Abstract This paper investigates numerical methods for simulations of the short-term behavior of a geothermal energy storage. Such simulations are needed for the optimal control and management of residential heating systems equipped with an underground thermal storage. There a given volume under or aside of a building is filled with soil and insulated to the surrounding ground. The thermal energy is stored by raising the temperature of the soil inside the storage. It is charged and discharged via pipe heat exchangers filled with a moving fluid. Simulations of geothermal energy storages aim to determine how much energy can be stored in or taken from the storage within a given short period of time. The latter depends on the dynamics of the spatial temperature distribution in the storage which is governed by a linear heat equation with convection and appropriate boundary and interface conditions. We consider semi- and full discretization of that PDE using finite difference schemes and study associated stability problems. Numerical results based on the derived methods are presented in the companion paper [17].

Keywords Geothermal storage · Mathematical modeling · Heat equation with convection · Finite difference discretization · Stability analysis

Mathematics Subject Classification (2010) 65M06 · 65M12 · 97M50

1 Introduction

Thermal storage facilities help to mitigate and to manage temporal fluctuations of heat supply and demand for heating and cooling systems of single buildings as well as for district heating systems. They allow heat to be stored in form of thermal energy and be used hours, days, weeks or months later. This is attractive for space heating, domestic or process hot water production, or generating electricity. Note that thermal energy may also be stored in the way of cold. Thermal storages can significantly increase both the

Paul Honore Takam

Brandenburg University of Technology Cottbus-Senftenberg, Institute of Mathematics, P.O. Box 101344, 03013 Cottbus, Germany; E-mail: takam@b-tu.de

Ralf Wunderlich

Brandenburg University of Technology Cottbus-Senftenberg, Institute of Mathematics, P.O. Box 101344, 03013 Cottbus, Germany; E-mail: ralf.wunderlich@b-tu.de

Olivier Menoukeu Pamen

University of Liverpool, Department of Mathematical Sciences, Liverpool L69 3BX, United Kingdom; E-mail: O.Menoukeu-Pamen@liverpool.ac.uk

flexibility and the performance of district energy systems and enhancing the integration of intermittent renewable energy sources into thermal networks (see Guelpa and Verda [8], Kitapbayev et al. [11]). Since heat production is still mainly based on burning fossil fuels (gas, oil, coal) these are important contributions for the reduction of carbon emissions and an increasing energy independence of societies.

For an overview on thermal energy storages we refer to Dincer and Rosen [6]. Zalba et al. [23] provides a review for the history of thermal energy storages with solid–liquid phase change and focused in three aspects: materials, heat transfer and applications. An overview of the European and in particular the Spanish thermal energy storage potential is presented in Arce et al. [1]. The authors show that thermal energy storages make an important contribution to the reduction of CO₂-emissions. In Soltani et al. [16] the authors provide a comprehensive review on the evolution of geothermal energy production from its beginnings to the present time by reporting production data from individual countries and collective data of worldwide production.

The efficient operation of geothermal storages requires a thorough design and planning because of the considerable investment cost. For that purpose, mathematical models and numerical simulations are widely used. We refer to Dahash et al. [5] and the references therein. In that paper the authors investigate large-scale seasonal thermal energy storages allowing for buffering intermittent renewable heat production in district heating systems. Numerical simulations are based on a multi-physics model of the thermal energy storage which was calibrated to measured data for a pit thermal energy storage in Dronninglund (Denmark). Another contribution is Major et al. [13] which considers heat storage capabilities of deep sedimentary reservoirs. The governing heat and flow equations are solved using finite element methods. Further, Regnier et al. [14] study the numerical simulation of aquifer thermal energy storages and focus on dynamic mesh optimisation for the finite element solution of the heat and flow equations. For further contributions to the numerical simulation of such storages we refer to [2, 6, 9, 12, 16, 22].

In this paper we focus on geothermal storages as depicted in Fig. 1.1. Such storages

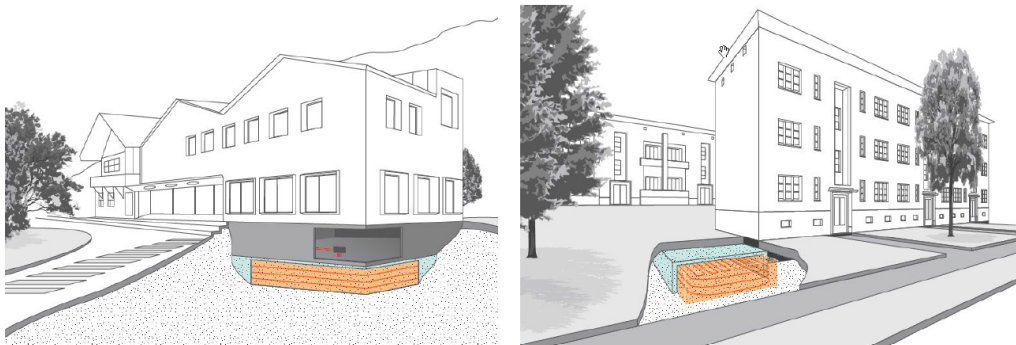


Fig. 1.1 Geothermal storage: in the new building, under a building (left) and in the renovation, aside of the building (right), see www.ezeit-ingenieure.eu, www.geo-ec.de.

gain more and more importance and are quite attractive for residential heating systems since construction and maintenance are relatively inexpensive. Furthermore, they can be integrated both in new buildings and in renovations. We will work with a 2D-model of a geothermal thermal energy storage, see Fig. 1.2, where a defined volume under or aside of a building is filled with soil and insulated to the surrounding ground. Thermal energy is stored by raising the temperature of the soil inside the storage. It is charged and discharged

via pipe heat exchangers (PHX) filled with some fluid (e.g. water). These PHXs can be connected to a short-term storage such as a water tank or directly to a solar collector and (heat) pumps move the fluid carrying the thermal energy. A special feature of the storage in this work is that it is not insulated at the bottom such that thermal energy can also flow into deeper layers as it can be seen in Fig. 1.2. This can be considered as a natural extension of the storage capacity since that heat can to some extent be retrieved if the storage is sufficiently discharged (cooled) and a heat flux back to storage is induced. Of course, there are unavoidable diffusive losses to the environment but due to the open architecture, the geothermal storage can benefit from higher temperatures in deeper layers of the ground and serve as a production unit similar to a downhole heat exchanger. Note that in many regions in Europe the temperature in a depth of only 10 meter is almost constant around 10°C over the year.

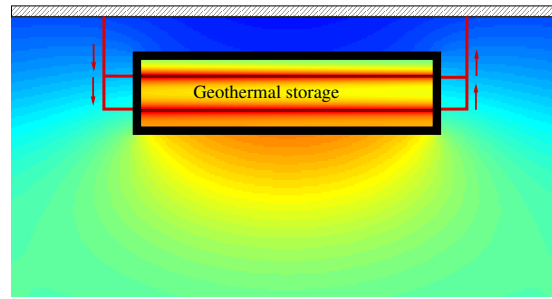


Fig. 1.2 2D-model of a geothermal storage insulated to the top and the sides while open at the bottom and spatial temperature distribution.

Geothermal storages enable an extremely efficient operation of heating and cooling systems in buildings. Further, they can be used to mitigate peaks in the electricity grid by converting electrical into heat energy (power to heat). Pooling several geothermal storages within the framework of a virtual power plant gives the necessary capacity which allows to participate in the balancing energy market.

This paper extends and complements the results in Bähr et al. [3,4] where the authors focus on the numerical simulation of the long-term behavior over weeks and months of the spatial temperature distribution in a geothermal storage and the interaction between a geothermal storage and its surrounding domain. For simplicity charging and discharging was described by a simple source term but not by PHXs.

In the present work we focus on the computation of the short-term behavior of the spatial temperature distribution. This is needed for storages embedded into residential heating systems and the study of the storage's response to charging and discharging operations on time scales from a few minutes to a few days. We extend the setting in [3,4] and include PHXs for a more realistic model of the storage's charging and discharging process. However, for the sake of simplicity we do not consider the surrounding medium but reduce the computational domain to the storage depicted in Fig. 1.2 by a black rectangle. Instead we set appropriate boundary conditions to mimic the interaction between storage and environment.

For the management and control of a storage which is embedded into a residential heating system one needs to know the amount of available thermal energy that can be stored in or extracted from the storage in a given short period of time. Such questions can only be answered if one knows the spatial temperature distribution, in particular around the PHXs. Charging and discharging is not efficient or even impossible if there are only small

differences between the temperatures inside and in the vicinity of the PHXs. Long periods of (dis)charging may lead to saturation in the vicinity of the PHXs. As a consequence (dis)charging is no longer efficient and should be stopped since propagation of heat to regions away from the PHXs takes time.

The short-term behavior of the spatial temperature distribution is governed by a linear heat equation with convection and appropriate boundary and interface conditions. We solve that PDE using finite difference schemes, see Duffy [7]. For the convection terms we apply upwind techniques. In a first step we study the semi-discretization with respect to spatial variables leading to a system of linear ODEs. In a second step, we consider full space-time discretization and derive implicit finite-difference schemes. The current paper provides the following theoretical contributions. First, we prove that the chosen semi-discretization ensures a system of linear ODEs with a stable system matrix. Second, we provide a detailed stability analysis for the implicit finite-difference schemes of the fully discretized PDE and establish a stability condition.

Numerical results are devoted to our companion paper [17]. There we perform extensive numerical experiments, where simulations results for the temporal behavior of the spatial temperature distribution are used to determine how much energy can be stored in or taken from the storage within a given short period of time. Special focus is laid on the dependence of these quantities on the arrangement of the PHXs within the storage. Further, we refer to another companion paper [18] in which we apply model reduction techniques known from control theory such as balanced truncation to derive low-dimensional approximations of aggregated characteristics of the temporal behavior of the spatial temperature distribution. The latter is crucial if the geothermal storage is embedded into a residential heating system and the cost-optimal management of such systems is studied mathematically in terms of optimal control problems.

The rest of the paper is organized as follows. In Sec. 2 we describe the dynamics of the spatial temperature distribution in the geothermal storage which is governed by a linear heat equation with a convection term and appropriate boundary and interface conditions. In Sec. 3 we present the semi-discretization with respect to spatial variables of the initial boundary value problem for that heat equation. For the resulting system of linear ODEs we show that the system matrix is stable. The full space-time discretization is studied in Sec. 4 where we derive implicit finite-difference schemes and provide the associated stability analysis. An appendix provides a list of frequently used notations, some technical details of the finite difference scheme, auxiliary results from matrix analysis as well as proofs which were removed from the main text.

2 Dynamics of Spatial Temperature Distribution in a Geothermal Storage

In this section we describe the dynamics of the spatial temperature distribution in a geothermal storage mathematically by a linear heat equation with convection term and appropriate boundary and interface conditions.

2.1 2D-Model

We assume that the domain of the geothermal storage is a cuboid and consider a two-dimensional rectangular cross-section. We denote by $Q = Q(t, x, y)$ the temperature at time

$t \in [0, T]$ in the point $(x, y) \in \mathcal{D} = (0, l_x) \times (0, l_y)$ with l_x, l_y denoting the width and height of the storage. The domain \mathcal{D} and its boundary $\partial\mathcal{D}$ are depicted in Fig. 2.1. \mathcal{D} is divided into three parts. The first is \mathcal{D}^M and is filled with a homogeneous medium (soil) characterized by constant material parameters ρ^M, κ^M and c_p^M denoting mass density, thermal conductivity and specific heat capacity, respectively. The second is \mathcal{D}^F , it represents the PHXs filled with a fluid (water) with constant material parameters ρ^F, κ^F and c_p^F . The fluid moves with time-dependent velocity $v_0(t)$ along the PHX. For the sake of simplicity we restrict ourselves to the case, often observed in applications, where the pumps moving the fluid are either on or off. Thus the velocity $v_0(t)$ is piecewise constant taking values $\bar{v}_0 > 0$ and zero, only. Finally, the third part is the interface \mathcal{D}^J between \mathcal{D}^M and \mathcal{D}^F . That interface is split into upper and lower interfaces $\overline{\mathcal{D}}^J$ and $\underline{\mathcal{D}}^J$, respectively. Observe that we neglect modeling the wall of the PHX and suppose perfect contact between the PHX and the soil. Details are given in (2.6) and (2.7) below. Summarizing we make the following

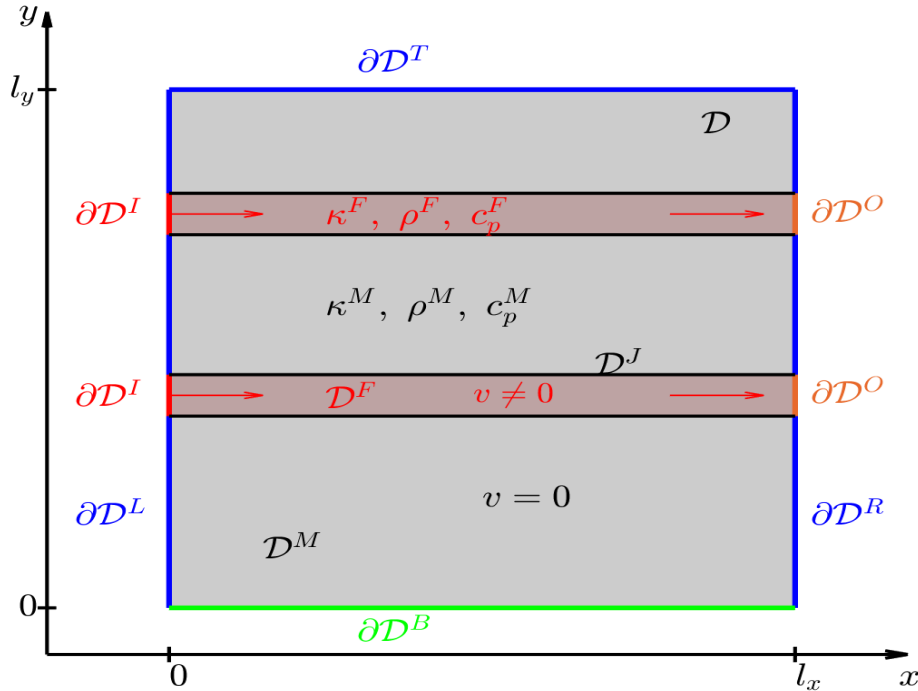


Fig. 2.1 2D-model of the geothermal storage: decomposition of the domain \mathcal{D} and the boundary $\partial\mathcal{D}$.

Assumption 2.1

1. Material parameters of the medium ρ^M, κ^M, c_p^M in the domain \mathcal{D}^M and of the fluid ρ^F, κ^F, c_p^F in the domain \mathcal{D}^F are constants.
2. Fluid velocity is piecewise constant, i.e. $v_0(t) = \begin{cases} \bar{v}_0 > 0, & \text{pump on,} \\ 0, & \text{pump off.} \end{cases}$
3. Perfect contact at the interface between fluid and medium.

Heat equation. The temperature $Q = Q(t, x, y)$ in the external storage is governed by the linear heat equation with convection term

$$\rho c_p \frac{\partial Q}{\partial t} = \nabla \cdot (\kappa \nabla Q) - \rho v \cdot \nabla (c_p Q), \quad (t, x, y) \in (0, T] \times \mathcal{D} \setminus \mathcal{D}^J,$$

where $\nabla = (\frac{\partial}{\partial x}, \frac{\partial}{\partial y})$ denotes the gradient operator. The first term on the right hand side describes diffusion while the second represents convection of the moving fluid in the PHXs. Further, $v = v(t, x, y) = v_0(t)(v^x(x, y), v^y(x, y))^T$ denotes the velocity vector with $(v^x, v^y)^T$ being the normalized directional vector of the flow. According to Assumption 2.1 the material parameters ρ, κ, c_p depend on the position (x, y) and take the values ρ^M, κ^M, c_p^M for points in \mathcal{D}^M (medium) and ρ^F, κ^F, c_p^F in \mathcal{D}^F (fluid).

Note that there are no sources or sinks inside the storage and therefore the above heat equation appears without forcing term. Based on this assumption, the heat equation (2.1) can be written as

$$\frac{\partial Q}{\partial t} = a\Delta Q - v \cdot \nabla Q, \quad (t, x, y) \in (0, T] \times \mathcal{D} \setminus \mathcal{D}^J, \quad (2.1)$$

where $\Delta = \frac{\partial^2}{\partial x^2} + \frac{\partial^2}{\partial y^2}$ is the Laplace operator and $a = a(x, y)$ is the thermal diffusivity which is piecewise constant with values $a^\dagger = \frac{\kappa^\dagger}{\rho^\dagger c_p^\dagger}$ with $\dagger = M$ for $(x, y) \in \mathcal{D}^M$ and $\dagger = F$ for $(x, y) \in \mathcal{D}^F$, respectively. The initial condition $Q(0, x, y) = Q_0(x, y)$ is given by the initial temperature distribution Q_0 of the storage.

Remark 2.2 In real-world geothermal storages PHXs are often designed in a snake form located in the storage domain at multiple horizontal layers. There may be only a single inlet and a single outlet. We will mimic that design by a computationally more tractable design characterized by multiple horizontal straight PHXs as it is sketched in Fig. 1.2. This allows to control the PHXs in different layers separately. For a topology with single inlet and outlet snake-shaped PHXs the outlet of a straight PHX in one layer can be connected with the inlet of the straight PHX in the next layer.

2.2 Boundary and Interface Conditions

For the description of the boundary conditions we decompose the boundary $\partial\mathcal{D}$ into several subsets as depicted in Fig. 2.1 representing the insulation on the top and the side, the open bottom, the inlet and outlet of the PHXs. Further, we have to specify conditions at the interface between PHXs and soil. The inlet, outlet and the interface conditions model the heating and cooling of the storage via PHXs. We distinguish between the two regimes 'pump on' and 'pump off'. For simplicity we assume perfect insulation at inlet and outlet if the pump is off. This leads to the following boundary conditions.

– *Homogeneous Neumann condition* describing perfect insulation on the top and the side

$$\frac{\partial Q}{\partial \mathbf{n}} = 0, \quad (x, y) \in \partial\mathcal{D}^T \cup \partial\mathcal{D}^L \cup \partial\mathcal{D}^R, \quad (2.2)$$

where $\partial\mathcal{D}^L = \{0\} \times [0, l_y] \setminus \partial\mathcal{D}^I$, $\partial\mathcal{D}^R = \{l_x\} \times [0, l_y] \setminus \partial\mathcal{D}^O$, $\partial\mathcal{D}^T = [0, l_x] \times \{l_y\}$ and \mathbf{n} denotes the outer-pointing normal vector.

– *Robin condition* describing heat transfer at the bottom

$$-\kappa^M \frac{\partial Q}{\partial \mathbf{n}} = \lambda^G (Q - Q^G(t)), \quad (x, y) \in \partial\mathcal{D}^B, \quad (2.3)$$

with $\partial\mathcal{D}^B = [0, l_x] \times \{0\}$, where $\lambda^G > 0$ denotes the heat transfer coefficient and $Q^G(t)$ the underground temperature. For more interpretation we refer to Remark 2.4.

- *Dirichlet condition* at the inlet if the pump is on ($v_0(t) > 0$), i.e. the fluid arrives at the storage with a given temperature $Q^I(t)$. If pump is off ($v_0(t) = 0$), we set a homogeneous Neumann condition describing perfect insulation.

$$\begin{cases} Q = Q^I(t), & \text{pump on,} \\ \frac{\partial Q}{\partial \mathbf{n}} = 0, & \text{pump off,} \end{cases} \quad (x, y) \in \partial \mathcal{D}^I. \quad (2.4)$$

- “*Do Nothing*” condition at the outlet in the following sense. If the pump is on ($v_0(t) > 0$) then the total heat flux directed outwards can be decomposed into a diffusive heat flux given by $\kappa^F \frac{\partial Q}{\partial \mathbf{n}}$ and a convective heat flux given by $v_0(t) \rho^F c_p^F Q$. Since in real-world applications the latter is much larger than the first we neglect the diffusive heat flux. This leads to a homogeneous Neumann condition

$$\frac{\partial Q}{\partial \mathbf{n}} = 0, \quad (x, y) \in \partial \mathcal{D}^O. \quad (2.5)$$

If the pump is off then we assume (as already for the inlet) perfect insulation which is also described by the above condition.

- *Smooth heat flux* at interface \mathcal{D}^J between fluid and soil leading to a coupling condition

$$\kappa^F \frac{\partial Q^F}{\partial \mathbf{n}} = \kappa^M \frac{\partial Q^M}{\partial \mathbf{n}}, \quad (x, y) \in \mathcal{D}^J. \quad (2.6)$$

Here, Q^F, Q^M denote the temperature of the fluid inside the PHX and of the soil outside the PHX, respectively. Moreover, we assume that the contact between the PHX and the medium is perfect which leads to a smooth transition of a temperature, i.e., we have

$$Q^F = Q^M, \quad (x, y) \in \mathcal{D}^J. \quad (2.7)$$

Remark 2.3 If the contact between the PHX and the medium is not perfect (e.g., in case of contact resistance) then the transition of the temperature at the interface \mathcal{D}^J will not be smooth, that is, $Q^F \neq Q^M$. This leads to a temperature jump between the PHX and the medium. That phenomenon occurs in the heat transfer between the medium and an insulation as shown in [3, 4].

Remark 2.4 Imposing the Robin condition (2.3) at the bottom boundary aims to mimic the thermal behavior at the bottom boundary. A more realistic description requires embedding the storage domain \mathcal{D} into a larger computational domain including the surrounding regions as in Fig. 1.2. This allows for warming and cooling in the vicinity of the storage resulting from the outflow and inflow of the storage heat. Contrary to that, condition (2.3) assumes an exogenously given underground temperature Q^G independent of the temperature in the storage.

The heat transfer coefficient λ^G describes the resistance to the heat flux at the boundary. For the limiting case $\lambda^G \rightarrow 0$ we get a homogeneous Neumann condition, i.e., perfect insulation, while in the limit for $\lambda^G \rightarrow \infty$ condition (2.3) is the Dirichlet condition $Q = Q^G(t)$. The underground temperature in general shows seasonal fluctuations which can be described by $Q^G(t) = K_1^G \cos\left(\frac{2\pi(t-t_0)}{T_a}\right) + K_2^G$, where K_1^G is the intensity of the fluctuation, K_2^G is the average ground temperature, t_0 a time or phase shift and T_a the number of time units per year. Since our focus is on the short-term behavior, we assume in the sequel that the underground temperature is constant over time, i.e. $K_1^G = 0$.

3 Semi-Discretization of the Heat Equation

This and the next section are devoted to the finite difference discretization of the heat equation (2.1) with the boundary and interface conditions (2.2) through (2.7). We proceed in two steps. In the first step we apply semi-discretization in space and approximate only spatial derivatives by their respective finite differences. This approach is also known as 'method of lines' and leads to a high-dimensional system of ODEs with a stable system matrix for the temperatures at the grid points. The latter will be used as starting point for model reduction in our paper [18]. In the second step, see Sec. 4, also time is discretized resulting in a family of implicit finite difference schemes for which we perform a stability analysis.

3.1 Semi-Discretization of the Heat Equation

We now apply the finite difference method (see Duffy [7]) combined with upwind techniques for the convection terms for semi-discretization of the heat equation (2.1).

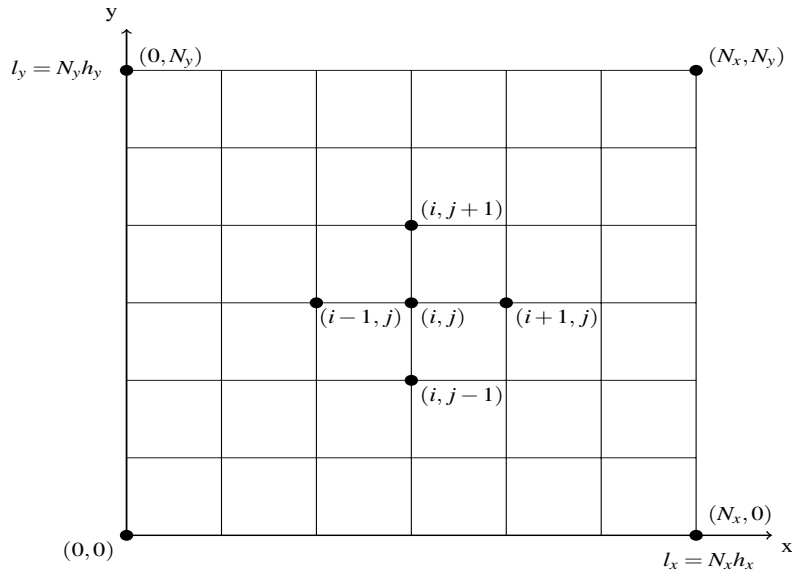


Fig. 3.1 Computational grid.

Let N_x and N_y be the number of grid points and $h_x = l_x/N_x$ and $h_y = l_y/N_y$ the step sizes in x -direction and y -direction, respectively. The spatial domain is discretized by means of a mesh with grid points (x_i, y_j) as shown in Fig. 3.1 where

$$x_i = ih_x, \quad y_j = jh_y, \quad i = 0, \dots, N_x, \quad j = 0, \dots, N_y.$$

We denote by $Q_{ij}(t) \simeq Q(t, x_i, y_j)$ the semi-discrete approximation of the temperature and by $v_0(t)(v_{ij}^x, v_{ij}^y)^\top = v_0(t)(v^x(x_i, y_j), v^y(x_i, y_j))^\top = v(t, x_i, y_j)$ the velocity vector at the grid point (x_i, y_j) at time t . Further, we introduce the following sets of indices

$$\begin{aligned} \mathcal{N}_x &= \{1, \dots, N_x - 1\}, \quad \mathcal{N}_y = \{1, \dots, N_y - 1\}, \\ \mathcal{N}^M &= \{(i, j) : (i, j) \in \mathcal{N}_x \times \mathcal{N}_y \text{ with } (x_i, y_j) \in \mathcal{D}^M\}, \end{aligned}$$

$$\begin{aligned}\mathcal{N}^F &= \{(i, j) : (i, j) \in \mathcal{N}_x \times \mathcal{N}_y \text{ with } (x_i, y_j) \in \mathcal{D}^F\}, \\ \mathcal{N}^J &= \{(i, j) : (i, j) \in \mathcal{N}_x \times \mathcal{N}_y \text{ with } (x_i, y_j) \in \mathcal{D}^J\}, \\ \mathcal{N}^B &= \{(i, j) : (i, j) \in \{0, \dots, N_x\} \times \{0, \dots, N_y\} \text{ with } (x_i, y_j) \in \partial\mathcal{D}\},\end{aligned}$$

which we identify with the corresponding sets of grid points. We denote by $\mathcal{N}^S = \mathcal{N}^F \cup \mathcal{N}^M$ the set of grid points in the inner domain $\mathcal{D}^S = \mathcal{D}^F \cup \mathcal{D}^M$. Further, we decompose the set of grid points on the interface $\mathcal{D}^J = \underline{\mathcal{D}}^J \cup \overline{\mathcal{D}}^J$ between the fluid and medium into $\mathcal{N}^J = \underline{\mathcal{N}}^J \cup \overline{\mathcal{N}}^J$. Here, $\underline{\mathcal{D}}^J$ and $\overline{\mathcal{D}}^J$ denote the lower and upper interface, respectively, see Fig. 2.1. Further, we decompose the set \mathcal{N}^B of grid points on the boundary domain $\partial\mathcal{D}$ according to the decomposition of $\partial\mathcal{D}$ given in Fig. 2.1 into $\mathcal{N}^B = \mathcal{N}_I^B \cup \mathcal{N}_O^B \cup \mathcal{N}_L^B \cup \mathcal{N}_R^B \cup \mathcal{N}_T^B \cup \mathcal{N}_B^B$.

The spatial derivatives in the PDE (2.1) are approximated by linear combinations of values of Q at the grid points (x_i, y_j) in \mathcal{D}^S at time t . We use central second-order finite difference for the diffusion term:

$$\begin{aligned}\frac{\partial^2 Q(t, x_i, y_j)}{\partial x^2} &= \frac{Q_{i+1,j}(t) - 2Q_{ij}(t) + Q_{i-1,j}(t)}{h_x^2} + \mathcal{O}(h_x^2), \\ \frac{\partial^2 Q(t, x_i, y_j)}{\partial y^2} &= \frac{Q_{i,j+1}(t) - 2Q_{ij}(t) + Q_{i,j-1}(t)}{h_y^2} + \mathcal{O}(h_y^2).\end{aligned}$$

For the convection term we use the upwind discretization to get

$$\begin{aligned}v^x(x_i, y_j) \frac{\partial Q(t, x_i, y_j)}{\partial x} &= v_{ij}^x \mathbb{1}_{\{v_{ij}^x > 0\}} \frac{Q_{ij}(t) - Q_{i-1,j}(t)}{h_x} \\ &\quad + v_{ij}^x \mathbb{1}_{\{v_{ij}^x < 0\}} \frac{Q_{i+1,j}(t) - Q_{ij}(t)}{h_x} + \mathcal{O}(h_x), \\ v^y(x_i, y_j) \frac{\partial Q(t, x_i, y_j)}{\partial y} &= v_{ij}^y \mathbb{1}_{\{v_{ij}^y > 0\}} \frac{Q_{ij}(t) - Q_{i,j-1}(t)}{h_y} \\ &\quad + v_{ij}^y \mathbb{1}_{\{v_{ij}^y < 0\}} \frac{Q_{i,j+1}(t) - Q_{ij}(t)}{h_y} + \mathcal{O}(h_y).\end{aligned}$$

We have to point out that the above upwind approximations of the convection terms need to be applied only to the set of grid points \mathcal{N}^F in the fluid domain \mathcal{D}^F , since there is no convection outside the fluid and we can set $v_{ij}^x = v_{ij}^y = 0$.

For the sake of simplification and tractability of our analysis we restrict ourselves to the following assumption on the arrangement of PHXs and impose conditions on the location of grid points along the PHXs.

Assumption 3.1

1. There are $n_P \in \mathbb{N}$ straight horizontal PHXs, the fluid moves in positive x -direction.
2. The interior of PHXs contains grid points.
3. Each interface between medium and fluid contains grid points.

Then for grid points in the domain \mathcal{D}^S the semi-discrete scheme is given by

$$\frac{dQ_{ij}(t)}{dt} = \alpha_{ij}^+(t)Q_{i+1,j}(t) + \alpha_{ij}^-(t)Q_{i-1,j}(t) + \beta_{ij}^+(t)Q_{i,j+1}(t) + \beta_{ij}^-(t)Q_{i,j-1}(t)$$

$$+ \gamma_{ij}(t) Q_{ij}(t). \quad (3.1)$$

For grid points $(i, j) \in \mathcal{N}^F$ in the “fluid” domain \mathcal{D}^F Assumption 3.1 implies that $v_{ij}^x = 1$ while $v_{ij}^y = 0$ and the above coefficients are given by

$$\begin{aligned} \alpha_{ij}^+(t) &= \alpha^{F+} = \frac{a^F}{h_x^2}, \quad \alpha_{ij}^-(t) = \alpha^{F-}(t) = \frac{a^F}{h_x^2} + \frac{v_0(t)}{h_x}, \quad \beta_{ij}^\pm(t) = \beta^F = \frac{a^F}{h_y^2}, \\ \gamma_{ij}(t) &= \gamma^F(t) = -2a^F \left(\frac{1}{h_x^2} + \frac{1}{h_y^2} \right) - \frac{v_0(t)}{h_x}, \quad \text{with } a^F = \frac{\kappa^F}{\rho^F c_p^F}. \end{aligned} \quad (3.2)$$

In the “medium” domain \mathcal{D}^M the convection terms disappear and the coefficients of the scheme (3.1) become time-independent and are given for $(i, j) \in \mathcal{N}^M$, by

$$\alpha_{ij}^\pm(t) = \alpha^M = \frac{a^M}{h_x^2}, \quad \beta_{ij}^\pm(t) = \beta^M = \frac{a^M}{h_y^2}, \quad \gamma_{ij}(t) = \gamma^M = -2a^M \left(\frac{1}{h_x^2} + \frac{1}{h_y^2} \right), \quad (3.3)$$

and $a^M = \frac{\kappa^M}{\rho^M c_p^M}$. Note that for the grid points in the neighborhood of the interfaces we have to slightly modify the above scheme (3.1) due to the extra contribution from the interfaces, see equations (3.8) and (3.9) below.

3.2 Semi-Discretization of the Boundary Conditions

In this paragraph we consider the discretization of boundary conditions. We start with the homogeneous Neumann conditions (2.2) and (2.5) for the top, left, right and the outlet boundary, where the normal vector \mathbf{n} is equal to $(0, 1)^\top, (-1, 0)^\top, (1, 0)^\top$ and $(1, 0)^\top$, respectively. Using first-order differences for the normal derivative we obtain for all $t \in [0, T]$

$$\begin{cases} Q_{iN_y}(t) = Q_{iN_y-1}(t) & \text{for } (i, N_y) \in \mathcal{N}_T^B, \\ Q_{0j}(t) = Q_{1j}(t) & \text{for } (0, j) \in \mathcal{N}_L^B, \\ Q_{N_x j}(t) = Q_{N_x-1j}(t) & \text{for } (N_x, j) \in \mathcal{N}_R^B \cup \mathcal{N}_O^B. \end{cases} \quad (3.4)$$

Next, we discretize the Robin condition (2.3) at the bottom boundary $\partial\mathcal{D}^B$. We have $\mathbf{n} = (0, -1)^\top$ such that for all grid points $(i, 0) \in \mathcal{N}_B^B$, we have for all $t \in [0, T]$

$$Q_{i0}(t) = \frac{\kappa^M}{\kappa^M + \lambda^G h_y} Q_{i1}(t) + \frac{\lambda^G h_y}{\kappa^M + \lambda^G h_y} Q^G(t). \quad (3.5)$$

On the inlet boundary $\partial\mathcal{D}^I$ we have according to (2.4) a Dirichlet boundary condition during pumping and a Neumann condition if the pump is off. Then for all grid points $(0, j) \in \mathcal{N}_I^B$, we have $\mathbf{n} = (-1, 0)^\top$ which implies for all $t \in [0, T]$

$$\begin{cases} Q_{0j}(t) = Q^I(t), & \text{if pump on,} \\ Q_{0j}(t) = Q_{1j}(t), & \text{if pump off.} \end{cases} \quad (3.6)$$

The relations (3.4) through (3.6) represent linear algebraic equations which allow to express the grid values $Q_{ij}(t)$ in the boundary grid points $(i, j) \in \mathcal{N}^B$ in terms of the corresponding values in the neighboring points in the interior of the domain and the input data to the boundary conditions. Thus, in the finite difference scheme these values $Q_{ij}(t)$ can be removed from the set of unknowns.

3.3 Semi-Discretization of Interface Condition

Now we consider grid points on the interface \mathcal{D}^J between fluid and medium which are by Assumption 2.1 straight lines in x -direction. That interface can be decomposed as $\mathcal{D}^J = \underline{\mathcal{D}}^J \cup \overline{\mathcal{D}}^J$, with $\underline{\mathcal{D}}^J$ and $\overline{\mathcal{D}}^J$ representing the lower and upper interface, respectively, see Fig. 3.2. We define the outer normal by $\mathbf{n} = (0, 1)^\top$ on the upper interface and by $\mathbf{n} =$

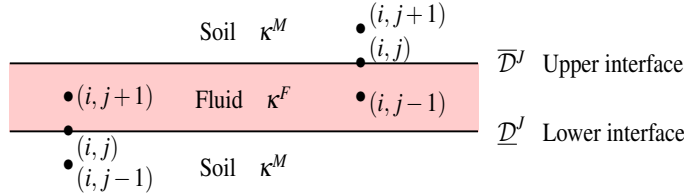


Fig. 3.2 Interface between the fluid and soil.

$(0, -1)^\top$ for lower interface. Note that we have n_P PHXs and each PHX has two interfaces. Then, we have in total $2n_P$ interface subdomains.

For a grid point (x_i, y_j) on the interface \mathcal{D}^J the perfect contact condition (2.7) implies that at a given time t the temperature of the fluid $Q^F(t, x_i, y_j)$ is equal to the temperature $Q^M(t, x_i, y_j)$ of the medium at that point. As usual, $Q_{ij}(t)$ denotes the semi-discrete approximation of that temperature. Then discretization of the interface condition (2.6) leads to

$$\begin{aligned} \kappa^F \frac{Q_{ij}(t) - Q_{i,j+1}(t)}{h_y} &= \kappa^M \frac{Q_{i,j-1}(t) - Q_{ij}(t)}{h_y} && \text{for lower interface} \\ \kappa^M \frac{Q_{i,j+1}(t) - Q_{ij}(t)}{h_y} &= \kappa^F \frac{Q_{ij}(t) - Q_{i,j-1}(t)}{h_y} && \text{for upper interface.} \end{aligned}$$

We obtain the following coupling between the grid values in an interface grid point $(i, j) \in \mathcal{N}^J$ and its neighbors in vertical direction a time $t \in [0, T]$,

$$\begin{aligned} Q_{ij}(t) &= \psi^F Q_{i,j+1}(t) + \psi^M Q_{i,j-1}(t), && (i, j) \in \underline{\mathcal{N}}^J, \\ Q_{ij}(t) &= \psi^F Q_{i,j-1}(t) + \psi^M Q_{i,j+1}(t), && (i, j) \in \overline{\mathcal{N}}^J, \\ \text{where } \psi^F &= \frac{\kappa^F}{\kappa^F + \kappa^M} \text{ and } \psi^M = 1 - \psi^F. \end{aligned} \quad (3.7)$$

The above relations show that the grid values $Q_{ij}(t)$ in the interface grid points $(i, j) \in \mathcal{N}^J$ can be expressed as linear combinations of the grid values in the two vertical neighboring points in the fluid and medium. Thus, in the finite difference scheme these values $Q_{ij}(t)$ can be removed from the set of unknowns. Now, let $(i, j) \in \underline{\mathcal{N}}^J$ be an interface point on the lower interface. Then substituting the above expressions for $Q_{ij}(t)$ into the finite differences scheme (3.1) applied to the lower neighbor $(i, j-1) \in \mathcal{N}^M$ in the medium leads to

$$\begin{aligned} \frac{d}{dt} Q_{i,j-1}(t) &= \alpha^M Q_{i+1,j-1}(t) + \alpha^M Q_{i-1,j-1}(t) + \beta^M Q_{i,j-2}(t) + \beta_I^M Q_{i,j+1}(t) + \gamma_I^M Q_{i,j-1}(t) \\ \text{with } \beta_I^M &= \psi^F \beta^M \text{ and } \gamma_I^M = \gamma + \psi^M \beta^M, \end{aligned} \quad (3.8)$$

whereas for the upper neighbor $(i, j+1) \in \mathcal{N}^F$ in the fluid it holds

$$\begin{aligned} \frac{d}{dt} Q_{i,j+1}(t) &= \alpha^{F+} Q_{i+1,j+1}(t) + \alpha^{F-} Q_{i-1,j+1}(t) + \beta^F Q_{i,j+2}(t) + \beta_I^F Q_{i,j-1}(t) + \gamma_I^F Q_{i,j+1}(t) \\ \text{with } \beta_I^F &= \psi^M \beta^F \quad \text{and} \quad \gamma_I^F = \gamma + \psi^F \beta^F. \end{aligned} \quad (3.9)$$

Similar expressions can be derived for points $(i, j) \in \overline{\mathcal{N}}^J$ on the upper interface.

3.4 Matrix Form of the Semi-Discrete Scheme

We are now in a position to establish a semi-discretized version of the heat equation (2.1) in terms of a system of ODEs by summarizing relations (3.1), (3.8) and (3.9). To this end we recall that the temperature at the boundary grid points can be obtained by the linear algebraic equations (3.4) through (3.6) derived from the boundary conditions. Further, the values at the interface points are obtained by the interpolation formulas in (3.7) derived from the perfect contact condition. Thus, we can exclude these grid points from the subsequent considerations where we collect the semi-discrete approximations of the temperature $Q(t, x_i, y_j)$ at the remaining points of the grid in the vector function $Y(t) = (Y_1(t), Y_2(t), \dots, Y_n(t))^T$. The enumeration of the entries of Y is such that we start with the first inner grid point $(1, 1)$ next to the lower left corner of the domain. Then we number grid points consecutively in vertical direction where we exclude the $2n_P$ points of the interfaces of the n_P PHXs such that we have $q = N_y - 2n_P - 1$ points in each ‘‘column’’ of the grid. Thus, $Y_{(i-1)q+1}$ corresponds to grid point $(i, 1)$ for $i = 1, \dots, N_x - 1$, and the last entry Y_n to the inner grid point $(N_x - 1, N_y - 1)$ next to the domain’s upper right corner. The dimension of Y is $n = (N_x - 1)q = (N_x - 1)(N_y - 2n_P - 1)$. The enumeration described above can be expressed formally by a mapping $\mathcal{K} : \mathcal{N}^{FM} \rightarrow \{1, \dots, n\}$ with $(i, j) \mapsto l = \mathcal{K}(i, j)$ which maps pairs of indices (i, j) of grid point $(x_i, y_j) \in \mathcal{D}$ to the single index l of the corresponding entry in the vector Y .

Using the above notations we can rewrite relations (3.1), (3.8) and (3.9) as the following system of ODEs for the vector function Y representing the semi-discretized heat equation (2.1) together with the given boundary and interface conditions.

$$\frac{dY(t)}{dt} = A(t)Y(t) + B(t)g(t), \quad t \in (0, T], \quad (3.10)$$

with the initial condition $Y(0) = y_0$. Here, the vector $y_0 \in \mathbb{R}^n$ contains the initial temperatures at the corresponding grid points with $y_{0l} = Q_0(x_i, y_j)$ where $l = \mathcal{K}(i, j)$, $l = 1, \dots, n$. The system matrix A results from the spatial discretization of the convection and diffusion term in the heat equation (2.1) together with the Robin and linear heat flux boundary conditions. It has tridiagonal structure consisting of $(N_x - 1) \times (N_x - 1)$ block matrices of dimension q given by

$$A = \begin{pmatrix} A_L & D^+ & & & 0 \\ D^- & A_M & D^+ & & \\ & D^- & A_M & D^+ & \\ & & \ddots & \ddots & \ddots \\ 0 & & & D^- & A_M & D^+ \\ & & & & D^- & A_R \end{pmatrix}. \quad (3.11)$$

The inner block matrices $A_M, i = 2, \dots, N_x - 2$ of dimension q have tridiagonal structure and are sketched for the case of one PHX in Table 3.1. The matrix entries β^F, γ^F are given in (3.2), β^M, γ^M in (3.3), β_I^M, γ_I^M in (3.8) and β_I^F, γ_I^F in (3.9). The first and last diagonal entry reads as $\gamma_B^M = \gamma^M + \frac{\kappa^M}{\kappa^M + \lambda^G h_y} \beta^M$, $\gamma_T^M = \gamma^M + \beta^M$, respectively. They are obtained if the discretized top and bottom boundary conditions (3.4) and (3.5) are substituted into (3.1).

For the matrices A_L and A_R containing entries resulting from the discretization of boundary conditions at the left and right boundary we refer to Appendix B. The lower

$$A_M = \left(\begin{array}{ccc} \gamma_B^M & \beta^M & \\ \beta^M & \gamma^M & \beta^M \\ & \ddots & \ddots \\ & \beta^M & \gamma^M & \beta^M \\ & \beta^M & \gamma_I^M & \beta_I^M \\ \hline & \beta_I^F & \gamma_I^F & \beta^F \\ & \beta^F & \gamma^F & \beta^F \\ & & \ddots & \ddots \\ & \beta^F & \gamma^F & \beta^F \\ \hline & \beta^F & \gamma_I^F & \beta_I^F \\ & \beta_I^M & \gamma_I^M & \beta^M \\ & \beta^M & \gamma^M & \beta^M \\ & & \ddots & \ddots & \ddots \\ & & \beta^M & \gamma^M & \beta^M \\ & & \beta^M & \gamma_T^M & \\ \hline \end{array} \right) \begin{array}{l} \text{Bottom Boundary} \\ \\ \text{Medium} \\ \\ \text{Lower interface} \\ \\ \\ \text{Fluid} \\ \\ \text{Upper interface} \\ \\ \text{Medium} \\ \text{Top Boundary} \end{array}$$

Table 3.1 Sketch of inner block matrices $A_M, i = 2, \dots, N_x - 2$ for the case of one PHX.

and upper block matrices $D^\pm \in \mathbb{R}^{q \times q}$, $i = 1, \dots, N_x - 1$, are diagonal matrices of the form

$$D^\pm = D^\pm(t) = \text{diag}(\alpha^M, \dots, \alpha^M | \alpha^{F^\pm}(t), \dots, \alpha^{F^\pm}(t) | \alpha^M, \dots, \alpha^M), \quad (3.12)$$

where α^M is given in (3.3) and $\alpha^{F\pm}$ in (3.2). Here, we denote by $|\cdot|$ the location of the interfaces where we only sketched the case of one PHX. For the convenience of the reader we provide a comprehensive list of all entries of matrix A showing the dependence on model and discretization parameters in Appendix D.

The $n \times 2$ input matrix B is a result from the discretization of the inlet and Robin boundary conditions, its entries B_{lr} , $l = 1, \dots, n$, $r = 1, 2$, are derived in Appendix B and are given by

$$\begin{aligned} B_{l1} = B_{l1}(t) &= \begin{cases} \frac{a^F}{h_x^2} + \frac{\bar{v}_0}{h_x}, & \text{pump on,} \\ 0, & \text{pump off,} \end{cases} & l = \mathcal{K}(1, j), (0, j) \in \mathcal{N}_I^{\mathcal{B}}, \\ B_{l2} &= \frac{\lambda^{G_{h_y}}}{\kappa^M + \lambda^{G_{h_y}}} \beta^M, & l = \mathcal{K}(i, 1), (i, 0) \in \mathcal{N}_B^{\mathcal{B}}. \end{aligned} \quad (3.13)$$

The entries for other l are zero. The input function $g: [0, T] \rightarrow \mathbb{R}^2$ is defined by

$$g(t) = \begin{cases} (Q^I(t), Q^G(t))^\top, & \text{pump on,} \\ (0, Q^G(t))^\top, & \text{pump off.} \end{cases} \quad (3.14)$$

Recall that Q^I is the inlet temperature of the PHX during pumping and Q^G is the underground temperature.

3.5 Stability of Matrix A

The finite difference semi-discretization of the heat equation (2.1) given by the system of ODEs (3.10) is expected to preserve the dissipativity of the PDE. This property is related to the stability of the system matrix $A = A(t)$ in the sense that all eigenvalues of A lie in the left open complex half plane. That property will play a crucial role for model reduction techniques for (3.10) based on balanced truncation in which we study in [18]. The next theorem confirms the expectations on the stability of A .

Theorem 3.2 (Stability of Matrix A)

Under Assumption 2.1 on the model and Assumption 3.1 on the discretization, the matrix $A = A(t)$ given in (3.11) is stable for all $t \in [0, T]$, i.e., all eigenvalues $\lambda(A)$ of A lie in left open complex half plane.

Proof Lemma D.2 in Appendix D shows by using Gershgorin's circle theorem, that the eigenvalues are either located in left open complex half plane or zero. Further, Lemma D.4 (also in Appendix D) shows that $A(t)$ is non-singular for all $t \in [0, T]$ and thus excludes the case $\lambda(A) = 0$. Thus, for all eigenvalues it holds $\lambda(A) \in \mathbb{C}_-$ and A is stable. \square

4 Full Discretization

After discretizing the heat equation (2.1) w.r.t. spatial variables we will now also discretize the temporal derivative and derive an explicit and a family of implicit finite difference schemes for which we perform a stability analysis.

4.1 θ -Implicit Finite Difference Scheme

We introduce the notation N_τ for the number of grid points in t -direction, $\tau = T/N_\tau$ the time step and $t_k = k\tau$, $k \in \mathcal{N}_\tau = \{0, \dots, N_\tau\}$. Let A^k, B^k, g^k, v_0^k be the values of $A(t), B(t), g(t), v_0(t)$ at time $t = t_k$, respectively. Further, we denote by $Y^k = (Y_1^k, \dots, Y_n^k)^\top$ the discrete-time approximation of the vector function $Y(t)$ at time $t = t_k$. Recall that Y contains the temperatures $Q = Q(t, x, y)$ at the points of the grid excluding points on the boundary and interface. Discretizing the temporal derivative in (3.10) with the forward difference gives

$$\frac{dY(t_k)}{dt} = \frac{Y^{k+1} - Y^k}{\tau} + \mathcal{O}(\tau). \quad (4.1)$$

Substituting (4.1) into (3.10) and replacing the r.h.s. of (3.10) by a convex combination of the values at time t_k and t_{k+1} with the weight $\theta \in [0, 1]$ gives the following general θ -implicit finite difference scheme

$$\frac{Y^{k+1} - Y^k}{\tau} = \theta[A(t_{k+1})Y^{k+1} + B(t_{k+1})g^{k+1}] + (1 - \theta)[A(t_k)Y^k + B(t_k)g^k]$$

from which we derive for $k = 0, \dots, N_\tau - 1$ the recursion

$$G^{k+1}Y^{k+1} = H^kY^k + \tau F^k \quad (4.2)$$

where $G^k = \mathbb{I}_n - \tau\theta A^k$, $H^k = \mathbb{I}_n + \tau(1 - \theta)A^k$, and $F^k = \theta B^{k+1}g^{k+1} + (1 - \theta)B^kg^k$,

with the initial value $Y^0 = Y(0)$ and the notation \mathbb{I}_n for the $n \times n$ identity matrix.

The above general θ -implicit scheme leads for $\theta = 1/2$ and 1 to special cases which are known in the literature as Crank-Nicolson scheme and backward Euler or fully implicit scheme, respectively. The limiting case $\theta = 0$ is not an implicit but a fully explicit scheme also known as forward Euler scheme.

4.2 Stability of the Finite Difference Scheme

In this subsection we investigate the stability of the finite difference scheme (4.2) in the maximum norm and present in Theorem 4.2 below a stability condition to the time discretization. The use of such stability results is twofold. First, it ensures “robustness” w.r.t. round-off errors of the problems’s input data, which are the initial condition and the inlet and underground temperature, in the sense that we can run the recursion for an arbitrarily long time without a total loss of accuracy. Second, stability of the scheme is a key ingredient in any analysis of convergence of the exact solution of the finite difference scheme to the exact solution of the given initial boundary value problem for the PDE for an infinite refinement of space and time discretization.

Note that a complete convergence analysis is beyond the scope of this paper. In particular, we do not investigate consistency issues. Consistency roughly says that the finite differences scheme approximates correctly the PDE. The proof of consistency is straightforward and based on Taylor series expansions. We refer to the Lax-Richtmyer Equivalence Theorem, see Sanz-Serna and Palencia [15], Thomas [19, Theorem 2.5.3], stating that a consistent finite difference scheme for a well-posed linear initial boundary value problem, is convergent if and only if it is stable. Hence, for a consistent scheme, convergence is synonymous with stability.

Our stability result is given in terms of maximum norms which are defined for a vector $X \in \mathbb{R}^n$ by $\|X\|_\infty = \max_{1 \leq i \leq n} |X_i|$ and for a square matrix $M \in \mathbb{C}^{n \times n}$ by $\|M\|_\infty = \max_{1 \leq i \leq n} \sum_{j=1}^n |M_{ij}|$.

Definition 4.1 (Stability of difference scheme in the maximum norm)

The finite difference scheme (4.2) is stable in the maximum norm if there exist constants $C_0, C_g > 0$ such that

$$\|Y^k\|_\infty \leq C_0 \|Y^0\|_\infty + C_g \max_{0 \leq j \leq k} \|g^j\|_\infty \text{ for } k = 1, 2, \dots, \mathcal{N}_\tau. \quad (4.3)$$

Theorem 4.2 (Stability of θ -implicit scheme)

Under Assumption 2.1 on the model and Assumption 3.1 on the discretization it holds

1. *For $\theta \in [0, 1)$, the semi-implicit finite difference scheme (4.2) is stable if the time step τ satisfies the condition*

$$\tau \leq \frac{1}{(1-\theta)\eta}, \quad \text{where} \quad \eta = 2 \max\{a^F, a^M\} \left(\frac{1}{h_x^2} + \frac{1}{h_y^2} \right) + \frac{\bar{v}_0}{h_x}. \quad (4.4)$$

2. *For $\theta = 1$, the fully implicit finite difference scheme (4.2) is unconditionally stable, i.e., stable for any $\tau > 0$.*

The constants C_0, C_g in (4.3) can be chosen as

$$C_0 = 1 \text{ and } C_g = C_B T \text{ where } C_B = \max \{ \|B^P\|_\infty, \|B^N\|_\infty \}. \quad (4.5)$$

The proof is based on the following lemma which is proven in Appendix E.

Lemma 4.3 *Under Assumption 2.1 on the model and Assumption 3.1 on the discretization it holds for all $k = 0, \dots, N_\tau - 1$ and $\theta \in [0, 1]$ that*

1. *the matrices G^{k+1} given in (4.2) are invertible and $\|(G^{k+1})^{-1}\|_\infty \leq 1$ with equality for $\theta = 0$;*
2. *the matrices H^k given in (4.2) satisfy $\|H^k\|_\infty \leq 1$ for all $\tau > 0$ if $\theta = 1$; and for $\tau \leq \frac{1}{(1-\theta)\eta}$ if $\theta \in [0, 1)$, where η is given in (4.4);*
3. *the vectors F^k given in (4.2) satisfy $\|F^k\|_\infty \leq C_B \max_{0 \leq j \leq k+1} \|g^j\|_\infty$ where C_B given in (4.5).*

Proof of Theorem 4.2. From the invertibility of G^k (see Lemma 4.3,1.) and the iteration of the recursion (4.2) we obtain for $k = 1, \dots, N_\tau$ the explicit representation

$$\begin{aligned} Y^k &= (G^k)^{-1} H^{k-1} Y^{k-1} + \tau (G^k)^{-1} F^{k-1} \\ &= (G^k)^{-1} H^{k-1} (G^{k-1})^{-1} H^{k-2} Y^{k-2} + \tau (G^k)^{-1} H^{k-1} (G^{k-1})^{-1} F^{k-2} + \tau (G^k)^{-1} F^{k-1} \\ &= \dots = \left(\prod_{j=1}^k (G^{k-j+1})^{-1} H^{k-j} \right) Y^0 + \tau \sum_{j=0}^{k-1} \left(\prod_{i=1}^j (G^{k-i+1})^{-1} H^{k-i} \right) (G^{k-j})^{-1} F^{k-j-1}, \end{aligned}$$

where we define $\prod_{j=1}^0 (\cdot) = \mathbb{I}_n$. Taking the maximum norm on both sides and applying the triangular and Cauchy-Schwarz inequality gives

$$\begin{aligned} \|Y^k\|_\infty &\leq \left(\prod_{j=1}^k \|(G^{k-j+1})^{-1}\|_\infty \|H^{k-j}\|_\infty \right) \|Y^0\|_\infty \\ &\quad + \tau \sum_{j=0}^{k-1} \left(\prod_{i=1}^j \|(G^{k-i+1})^{-1}\|_\infty \|H^{k-i}\|_\infty \right) \|(G^{k-j})^{-1}\|_\infty \|F^{k-j-1}\|_\infty. \end{aligned}$$

Substituting the estimates for $\|(G^k)^{-1}\|_\infty, \|H^k\|_\infty$ and $\|F^k\|_\infty$ given in Lemma 4.3 into the above inequality yields

$$\|Y^k\|_\infty \leq \|Y^0\|_\infty + \tau k C_B \max_{0 \leq j \leq k} \|g^j\|_\infty \leq \|Y^0\|_\infty + C_B T \max_{0 \leq j \leq k} \|g^j\|_\infty,$$

where we used $\tau k \leq \tau N_\tau = T$. According to the second assertion of Lemma 4.3 the above estimate holds for all $\tau > 0$ if $\theta = 1$ and for $\tau \leq \frac{1}{(1-\theta)\eta}$ if $\theta \in [0, 1)$. \square

5 Conclusion

We have investigated numerical methods for the simulation of the short-term behavior of the spatial temperature distribution in a geothermal energy storage. The underlying initial

boundary value problem for the heat equation with a convection term has been discretized using finite difference schemes. In a first step we studied the semi-discretization with respect to spatial variables. For the resulting system of linear ODEs we proved that the system matrix is stable. In a second step the full space-time discretization has been considered. Here we derived explicit and implicit finite-difference schemes and investigated associated stability problems.

Based on the findings of this paper we present in [17] results of a large number of numerical experiments where we have shown how these simulations can support the design and operation of a geothermal storage. Examples are the dependence of the charging and discharging efficiency on the topology and arrangement of PHXs and on the length of charging and discharging periods.

In [18] we study model reduction techniques to derive low-dimensional approximations of aggregated characteristics of the temperature distribution describing the input-output behavior of the storage. The latter is crucial if the geothermal storage is embedded into a residential heating system and the cost-optimal management of such systems is studied mathematically in terms of optimal control problems.

A List of Notations

| | |
|--|---|
| $Q = Q(t, x, y)$ | temperature in the geothermal storage |
| T | finite time horizon |
| l_x, l_y, l_z | width, height and depth of the storage |
| $\mathcal{D} = (0, l_x) \times (0, l_y)$ | domain of the geothermal storage |
| $\mathcal{D}^M, \mathcal{D}^F$ | domain of medium (soil) and PHX fluid |
| $\mathcal{D}^J = \underline{\mathcal{D}}^J \cup \overline{\mathcal{D}}^J$ | interface between the PHXs and the medium |
| $\partial \mathcal{D}$ | boundary of the domain |
| $\partial \mathcal{D}^I, \partial \mathcal{D}^O$ | inlet and outlet boundaries of the PHX |
| $\partial \mathcal{D}^L, \partial \mathcal{D}^R, \partial \mathcal{D}^T, \partial \mathcal{D}^B$ | left, right, top and bottom boundaries of the domain |
| $\mathcal{N}^M, \mathcal{N}^F$ | subset of index pairs of points in the medium and PHX fluid |
| $\mathcal{N}^J, \underline{\mathcal{N}}^J, \overline{\mathcal{N}}^J, \mathcal{N}_*^B$ | subsets of index pairs for points on interface and boundary |
| \mathcal{K} | mapping $(i, j) \mapsto l = \mathcal{K}(i, j)$ of index pairs to single indices |
| $v = v_0(t)(v^x, v^y)^\top$ | time-dependent velocity vector, |
| \bar{v}_0 | constant velocity during pumping |
| c_p^F, c_p^M | specific heat capacity of the fluid and medium |
| ρ^F, ρ^M | mass density of the fluid and medium |
| κ^F, κ^M | thermal conductivity of the fluid and medium |
| a^F, a^M | thermal diffusivity of the fluid and medium |
| λ^G | heat transfer coefficient between storage and underground |
| Q_0 | initial temperature distribution of the geothermal storage |
| $Q^G(t)$ | underground temperature |
| $Q^I(t), Q_C^I(t), Q_D^I(t)$ | inlet temperature of the PHX, during charging and discharging, |
| N_x, N_y, N_τ | number of grid points in x, y and τ -direction |
| h_x, h_y, τ | step size in x and y -direction and the time step |
| \mathbf{n} | outward normal to the boundary $\partial \mathcal{D}$ |
| n | dimension of vector Y |
| n_P | number of PHXs |
| \mathbb{I}_n | $n \times n$ identity matrix |
| A | $n \times n$ dimensional system matrix |
| B | $n \times m$ dimensional input matrix |
| D^\pm, A_L, A_M, A_R | block matrices of matrix A |
| q | dimension of block matrices |
| $\alpha_*, \beta_*, \gamma_*$ | coefficients of the matrix A |
| ψ^F, ψ^M | weighting factors for discretization of interface condition |
| Y | vector of temperatures at grid points |
| g | input variable of the system |
| $\nabla, \Delta = \nabla \cdot \nabla$ | gradient, Laplace operator |
| PHX | pipe heat exchanger |

B Block Matrices A_L and A_R

This appendix gives the first and the last diagonal block matrices A_L and $A_R \in \mathbb{R}^{q \times q}$ of the matrix A given in (3.11). Its entries result from the discretization of boundary conditions at the left and right boundary. Both block matrices are tridiagonal and sketched for the case of only one PHX in Table B.1. The entries in the first and last row are related to the inner grid points next to the four corners of the domain and obtained by substituting homogeneous Neumann condition (3.4) and

Table B.1 Sketch of the matrices A_L and A_R for the case of one PHX.

$$\begin{aligned} \frac{d}{dt}Q_{11}(t) &= \alpha^M Q_{21}(t) + \alpha^M Q_{01}(t) + \beta^M Q_{12}(t) + \beta^M Q_{10}(t) + \gamma^M Q_{11}(t) \\ &= \alpha^M Q_{21}(t) + \beta^M Q_{12}(t) + \left(\alpha^M + \frac{\kappa^M}{\kappa^M + \lambda^G h_y} \beta^M + \gamma^M \right) Q_{11}(t) + \frac{\lambda^G h_y}{\kappa^M + \lambda^G h_y} \beta^M Q^G(t) \\ &= \alpha^M Q_{21}(t) + \beta^M Q_{12}(t) + \gamma_{BB}^M Q_{11}(t) + \frac{\lambda^G h_y}{\kappa^M + \lambda^G h_y} \beta^M Q^G(t), \end{aligned}$$

Analogously, we derive for the lower right corner

Note that the last terms on the r.h.s. of the above equations are contributions to the input term $B(t)g(t)$ given in (3.13) and (3.14). For the grid points next to the upper left and right corner we have to apply the homogeneous Neumann conditions (3.4) and obtain from (3.1)

where $\gamma_{TB}^M = \alpha^M + \beta^M + \gamma^M$. Analogously, we derive for the upper right corner

For “inner” grid points located next to insulated left and right boundary but not next to the upper and lower boundary or the interface we have to combine (3.1) with the homogeneous Neumann condition (3.4). This leads to the coefficient $\gamma_B^M = \gamma^M + \alpha^M$ on the main diagonal.

For the grid points next to the inlet boundary we apply Dirichlet condition during pumping and homogeneous Neumann condition if the pump is off, see (3.6). For j with $(0, j) \in \mathcal{N}_I^B$ it holds

$$\begin{aligned} \frac{d}{dt} Q_{1j}(t) &= \alpha^{F+} Q_{2j}(t) + \alpha^{F-} Q_{0j}(t) + \beta^F Q_{1,j+1}(t) + \beta^F Q_{1,j-1}(t) + \gamma^F Q_{1j}(t) \\ &= \alpha^{F+} Q_{2j}(t) + \beta^F Q_{1,j+1}(t) + \beta^F Q_{1,j-1}(t) + \begin{cases} \gamma^F Q_{1j}(t) + \alpha^{F-} Q^I(t) & \text{pump on} \\ (\gamma^F + \alpha^{F-}) Q_{1j}(t) & \text{pump off} \end{cases} \\ &= \alpha^{F+} Q_{2j}(t) + \beta^F Q_{1,j+1}(t) + \beta^F Q_{1,j-1}(t) + \gamma_L^F Q_{1j}(t) + b_{k1} Q^I(t), \end{aligned}$$

where $\gamma_L^F = \gamma_L^F(t) = \begin{cases} \gamma^F & \text{pump on,} \\ \gamma^F + \frac{\alpha^F}{h_x^2} & \text{pump off,} \end{cases}$ and $B_{l1} = B_{l1}(t) = \begin{cases} \frac{\alpha^F}{h_x^2} + \frac{\bar{v}_0}{h_x} & \text{pump on,} \\ 0 & \text{pump off,} \end{cases}$

with $l = \mathcal{K}(1, j)$. We note that $\alpha^{F\pm}, \beta^F, \gamma^F$ are given in (3.2) and point out that the term $b_{k1} Q^I(t)$ contributes to the input term $B(t)g(t)$.

At the outlet boundary we have homogeneous Neumann condition and for the grid points next to the outlet we obtain from the discretized boundary condition (3.4) for j with $(N_x, j) \in \mathcal{N}_O^B$ it holds

$$\begin{aligned} \frac{d}{dt} Q_{N_x-1,j}(t) &= \alpha^{F+} Q_{N_x,j}(t) + \alpha^{F-} Q_{N_x-2,j}(t) + \beta^F Q_{N_x-1,j+1}(t) + \beta^F Q_{N_x-1,j-1}(t) + \gamma^F Q_{N_x-1,j}(t) \\ &= \alpha^{F-} Q_{N_x-2,j}(t) + \beta^F Q_{N_x-1,j+1}(t) + \beta^F Q_{N_x-1,j-1}(t) + \gamma_R^F Q_{N_x-1,j}(t), \end{aligned}$$

where $\gamma_R^F = \gamma^F + \alpha^{F+}$ and $\alpha^{F\pm}, \beta^F, \gamma^F$ are given in (3.2).

Finally, for the grid points next to the interface we obtain by an analogous procedure as described in Subsec. 3.3 the coefficients

$$\gamma_{IB}^M = \gamma_B^M + \psi^M \beta^M, \quad \gamma_{IL}^F = \gamma_L^F(t) = \gamma_L^F(t) + \psi^F \beta^F, \quad \gamma_{IR}^F = \gamma_R^F + \psi^F \beta^F,$$

where ψ^M and ψ^F are given (3.7). Recall that the off-diagonal coefficients β_I^M, β_I^F are given in (3.8), (3.9).

C Auxiliary Results From Matrix Analysis

In this appendix we collect some results from matrix analysis taken from the literature. They will be used in the proofs of Theorem 3.2 and Lemma 4.3. Let $M \in \mathbb{C}^{n \times n}$ be some generic matrix. For $i = 1, \dots, n$ we introduce the notations

$$R_i(M) = \sum_{j \neq i} |M_{ij}|, \quad J_i(M) = |M_{ii}| - R_i(M), \quad S_i(M) = |M_{ii}| + R_i(M) = \sum_j |M_{ij}|. \quad (\text{C.1})$$

Note that the maximum norm of M is given by $\|M\|_\infty = \max_i S_i(M)$. The quantities $R_i(M)$ appear as radii of Gershgorin's circles of M and the $J_i(M)$ are used to describe diagonal dominance of M .

Lemma C.1 (Gershgorin's Circle Theorem, Varga [21])

Let $M \in \mathbb{C}^{n \times n}$ and for $i = 1, \dots, n$ let $D_i = \{z \in \mathbb{C} : |z - M_{ii}| \leq R_i\}$ be the closed discs in the complex plane centred at M_{ii} with radius $R_i = R_i(M)$ given in (C.1). Then all the eigenvalues of M lie in the union of the discs D_1, \dots, D_n .

Definition C.2 (Diagonal Dominance)

Row $i \in \{1, \dots, n\}$ of a matrix $M \in \mathbb{C}^{n \times n}$ is called *strictly diagonal dominant* if $J_i(M) > 0$,
weakly diagonal dominant if $J_i(M) \geq 0$,

The matrix M is called *strictly (weakly) diagonal dominant* if all of its rows are strictly (weakly) diagonal dominant.

The following result says that strictly diagonal dominant matrices are invertible and provides a upper bound for the maximum norm of the inverse.

Lemma C.3 (Varah [20], Theorem 1)

Let $M \in \mathbb{C}^{n \times n}$ strictly diagonal dominant matrix. Then M is invertible and

$$\|M^{-1}\|_{\infty} \leq \frac{1}{J(M)}, \quad \text{where} \quad J(M) = \min_{1 \leq i \leq n} J_i(M).$$

Matrices which are weakly but not strictly diagonal dominant can be singular. A criterion for non-singularity is based on the following property of a matrix and the subsequent lemma. That property was introduced in Horn and Johnson [10, Definition 6.2.7] and termed “property SC”. In the literature it is also known as “strongly connected”.

Definition C.4 (Strongly Connected Matrix)

A matrix $M \in \mathbb{C}^{n \times n}$ is called strongly connected (or of property SC) if for each pair of distinct integers $p, q \in \{1, \dots, n\}$ there is a sequence of distinct integers $k_1 = p, k_2, \dots, k_m = q$ such that each entry $M_{k_1 k_2}, M_{k_2 k_3}, \dots, M_{k_{m-1} k_m}$ is non-zero.

For strongly connected matrices Horn and Johnson [10, Corollary 6.2.9] give the following criterion for non-singularity.

Lemma C.5 (Better’s Corollary)

Suppose that the matrix $M \in \mathbb{C}^{n \times n}$ is strongly connected, weakly diagonally dominant and there exists one strictly diagonal dominant row. Then M is nonsingular.

D Properties of Matrix A

We recall that the time-dependence of $A(t)$ is a result of the discretization of convection terms in the heat equation (2.1). The latter depend on the time-dependent velocity $v_0(t)$ and with some abuse of notation we can write $A = A(t) = A(v_0(t))$ and $B = B(t) = B(v_0(t))$. Recall that we assume in Ass. 2.1 that $v_0(t)$ is piecewise constant with $v_0(t) = \bar{v}_0$ during charging and discharging when the pump is on whereas $v_0(t) = 0$ if the pump is off. Therefore, the matrices A, B share this property. They take only the two values $A^P = A(\bar{v}_0)$, $B^P = B(\bar{v}_0)$ during pumping and $A^N = A(0)$, $B^N = B(0)$ if the pump is off. Thus, for studying properties of $A(t)$ on $[0, T]$ or of $A^k = A(k\tau)$ for $k = 0, \dots, N_\tau$ it is sufficient to look at the properties of A^P and A^N .

We want to have a closer look to the entries of the block matrices A_M, A_L, A_R given in Tables 3.1, B.1 and of D^\pm given in (3.12), forming the system matrix A . It turns out that for the diagonal entries and the row characteristics R_i, J_i, S_i given in (C.1) one has to distinguish 14 different cases. Instead of n rows it is sufficient to consider only 14 representative rows whose indices we denote by $i_l, l = 1, \dots, 14$. Table D.1 provides a list of diagonal entries $A_{i_l i_l}$ and the row characteristics $R_{i_l}(A), J_{i_l}(A), S_{i_l}(A)$ in terms of the model and discretization parameters. For the convenience of the reader we give below that information also for the individual non-diagonal entries of A .

$$\begin{aligned} \beta^M &= \frac{a^M}{h_y^2}, \quad \beta^F = \frac{a^F}{h_y^2}, \quad \beta_l^F = \frac{\kappa^F}{\kappa^F + \kappa^M} \beta^M, \quad \beta_l^F = \frac{\kappa^M}{\kappa^F + \kappa^M} \beta^F, \\ \alpha^M &= \frac{a^M}{h_x^2}, \quad \alpha^{F+} = \frac{a^F}{h_x^2}, \quad \alpha^{F-} = \frac{a^F}{h_x^2} + \frac{\bar{v}_0}{h_x}. \end{aligned}$$

Lemma D.1 The matrix $A = A(t)$ is weakly diagonal dominant for all $t \in [0, T]$.

Proof Inspecting the quantities $J_{i_l}(A)$ and Table D.1 it can be seen that it holds $J_{i_l}(A) \geq 0$, hence by Definition C.2 the matrix is diagonal dominant.

Note that A is weakly but not strictly diagonal dominant since not all of its rows are strictly diagonal dominant.

Lemma D.2 *The Gershgorin circles of the matrix $A = A(t)$ are subsets of $\mathbb{C}_- \cup \{0\}$ for all $t \in [0, T]$. Here, \mathbb{C}_- denotes the set of complex numbers with negative real part.*

Proof Let us examine the Gershgorin's circles of A for the 14 different representative rows denoted by $D_{i_l} = D_{i_l}(C_{i_l}, R_{i_l})$ with centres $C_{i_l} = A_{i_l i_l}$ and the radii $R_{i_l}(A)$, $l = 1, \dots, 14$, given in Table D.1. Since all entries of A are real, the centres $C_{i_l} = A_{i_l i_l} < 0$ of the discs are on the negative real axis. Lemma D.1 shows that A is diagonal dominant, i.e., $J_{i_l}(A) = |C_{i_l}| - R_{i_l}(A) \geq 0$. Hence, the radii $R_{i_l}(A)$ of the Gershgorin circles never exceed $|C_{i_l}|$ and it holds $D_{i_l} \subset \mathbb{C}_- \cup \{0\}$. \square

Lemma D.3 *The matrix $A = A(t)$ is strongly connected for all $t \in [0, T]$.*

Proof Let (p, q) be a pair of distinct integers with $p, q \in \{1, \dots, n\}$. Then we can choose the sequence of distinct integers k_1, k_2, \dots, k_m , such that $m = |p - q| + 1$ and $k_j = p + j - 1$ (for $p < q$) and $k_j = p - j + 1$ (for $p > q$). It holds $A_{k_j k_{j+1}} \neq 0$ since these entries are located on the upper and lower subdiagonal of A for which we have

$$A_{k_j k_{j+1}} = \begin{cases} \beta^{F/M}, & \text{for } (k_j, k_{j+1}) \in \mathcal{N}^{FM} \setminus \mathcal{N}_N^J, \\ \beta_I^{F/M}, & \text{for } (k_j, k_{j+1}) \in \mathcal{N}_N^J, \end{cases}$$

where \mathcal{N}^{FM} is the set of grid points in the fluid and medium $\mathcal{D}^F \cup \mathcal{D}^M$ and \mathcal{N}_N^J the set of neighboring grid points to the interface. Since $\beta^{F/M}$ given in (3.2), (3.3) and $\beta_I^{F/M}$ given in (3.8), (3.9) are positive, we have $A_{k_j k_{j+1}} \neq 0$, $j = 1, 2, \dots, m$. Thus, the matrix A is strongly connected. \square

Lemma D.4 *The matrix $A = A(t)$ is non-singular for all $t \in [0, T]$.*

Proof From Lemma D.1 and D.3 it is known that $A(t)$ is weakly diagonal dominant and strongly connected for all $t \in [0, T]$. Table D.1 shows that there exist strictly diagonal dominant rows. Hence, Better's Corollary (see Lemma C.5) implies that $A(t)$ is nonsingular. \square

Lemma D.5 *For the maximum norm of the matrix $A = A(t)$ it holds*

$$\max_{t \in [0, T]} \|A(t)\|_\infty = \max \{ \|A^P\|_\infty, \|A^N\|_\infty \} \leq 4 \max \{ a^F, a^M \} \left(\frac{1}{h_x^2} + \frac{1}{h_y^2} \right) + \frac{2\bar{v}_0}{h_x}.$$

Proof $A(t)$ is piecewise constant taking only the two values A^P and A^N . From the last column of Table D.1 showing the 14 different row sums $S_i(A^{P/N})$ of the two matrices it can be easily seen that $\|A^{P/N}\|_\infty \leq \max \{ S_{i_6}(A^{P/N}), S_{i_7}(A^{P/N}) \}$ yielding the estimate in the lemma. \square

| l | Gershgorin circles: centres $C_{i_l} = A_{i_l i_l}$ (diagonal entries) | Gershgorin circles: radii $R_{i_l}(A) = \sum_{j=1, j \neq i_l}^n A_{i_l, j} $ | Differences $J_{i_l}(A) = A_{i_l i_l} - \sum_{j=1, j \neq i_l}^n A_{i_l, j} $ | Row sums $S_{i_l}(A) = \sum_{j=1}^n A_{i_l, j} $ |
|-----|--|---|---|---|
| 1 | $-a^M \left(\frac{1}{h_x^2} + \frac{1}{h_y^2} \right) - \left(\frac{\lambda^G h_y}{\kappa^M + \lambda^G h_y} \right) \frac{a^M}{h_y^2}$ | $a^M \left(\frac{1}{h_x^2} + \frac{1}{h_y^2} \right)$ | $\left(\frac{\lambda^G h_y}{\kappa^M + \lambda^G h_y} \right) \frac{a^M}{h_y^2}$ | $2a^M \left(\frac{1}{h_x^2} + \frac{1}{h_y^2} \right) + \left(\frac{\lambda^G h_y}{\kappa^M + \lambda^G h_y} \right) \frac{a^M}{h_y^2}$ |
| 2 | $-a^M \left(\frac{1}{h_x^2} + \frac{1}{h_y^2} \right)$ | $a^M \left(\frac{1}{h_x^2} + \frac{1}{h_y^2} \right)$ | 0 | $2a^M \left(\frac{1}{h_x^2} + \frac{1}{h_y^2} \right)$ |
| 3 | $-a^M \left(\frac{2}{h_x^2} + \frac{1}{h_y^2} \right) - \left(\frac{\lambda^G h_x}{\kappa^M + \lambda^G h_x} \right) \frac{a^M}{h_x^2}$ | $a^M \left(\frac{2}{h_x^2} + \frac{1}{h_y^2} \right)$ | $\left(\frac{\lambda^G h_x}{\kappa^M + \lambda^G h_x} \right) \frac{a^M}{h_x^2}$ | $2a^M \left(\frac{2}{h_x^2} + \frac{1}{h_y^2} \right) + \left(\frac{\lambda^G h_x}{\kappa^M + \lambda^G h_x} \right) \frac{a^M}{h_x^2}$ |
| 4 | $-a^M \left(\frac{2}{h_x^2} + \frac{1}{h_y^2} \right)$ | $a^M \left(\frac{2}{h_x^2} + \frac{1}{h_y^2} \right)$ | 0 | $2a^M \left(\frac{2}{h_x^2} + \frac{1}{h_y^2} \right)$ |
| 5 | $-a^M \left(\frac{1}{h_x^2} + \frac{2}{h_y^2} \right)$ | $a^M \left(\frac{1}{h_x^2} + \frac{2}{h_y^2} \right)$ | 0 | $2a^M \left(\frac{1}{h_x^2} + \frac{2}{h_y^2} \right)$ |
| 6 | $-2a^M \left(\frac{1}{h_x^2} + \frac{1}{h_y^2} \right)$ | $2a^M \left(\frac{1}{h_x^2} + \frac{1}{h_y^2} \right)$ | 0 | $4a^M \left(\frac{1}{h_x^2} + \frac{1}{h_y^2} \right)$ |
| 7 | $-2a^F \left(\frac{1}{h_x^2} + \frac{1}{h_y^2} \right) - \frac{v_0(t)}{h_x}$ | $2a^F \left(\frac{1}{h_x^2} + \frac{1}{h_y^2} \right) + \frac{v_0(t)}{h_x}$ | 0 | $4a^F \left(\frac{1}{h_x^2} + \frac{1}{h_y^2} \right) + \frac{2v_0(t)}{h_x}$ |
| 8 | $\begin{cases} -2a^F \left(\frac{1}{h_x^2} + \frac{1}{h_y^2} \right) - \frac{\bar{v}_0}{h_x}, & A = A^P \\ -a^F \left(\frac{1}{h_x^2} + \frac{2}{h_y^2} \right), & A = A^N \\ -a^F \left(\frac{1}{h_x^2} + \frac{2}{h_y^2} \right) - \frac{v_0(t)}{h_x} \end{cases}$ | $\begin{cases} a^F + \frac{\bar{v}_0}{h_x}, & A = A^P \\ 0, & A = A^N \end{cases}$ | $\begin{cases} a^F + \frac{\bar{v}_0}{h_x}, & A = A^P \\ 0, & A = A^N \end{cases}$ | $\begin{cases} a^F \left(\frac{3}{h_x^2} + \frac{4}{h_y^2} \right) + \frac{\bar{v}_0}{h_x}, & A = A^P \\ 2a^F \left(\frac{1}{h_x^2} + \frac{2}{h_y^2} \right), & A = A^N \\ 2a^F \left(\frac{1}{h_x^2} + \frac{2}{h_y^2} \right) + \frac{2v_0(t)}{h_x} \end{cases}$ |
| 9 | $-a^F \left(\frac{1}{h_x^2} + \frac{2}{h_y^2} \right) - \frac{v_0(t)}{h_x}$ | $a^F \left(\frac{1}{h_x^2} + \frac{2}{h_y^2} \right) + \frac{v_0(t)}{h_x}$ | 0 | $2a^F \left(\frac{1}{h_x^2} + \frac{2}{h_y^2} \right) + \frac{2v_0(t)}{h_x}$ |
| 10 | $-a^M \left(\frac{2}{h_x^2} + \frac{1}{h_y^2} \right) - \left(\frac{\kappa^F}{\kappa^M + \kappa^F} \right) \frac{a^M}{h_y^2}$ | $\frac{2a^M}{h_x^2} + \left(1 + \frac{\kappa^F}{\kappa^M + \kappa^F} \right) \frac{a^M}{h_y^2}$ | 0 | $2a^M \left(\frac{2}{h_x^2} + \frac{1}{h_y^2} \right) + \left(\frac{2\kappa^F}{\kappa^M + \kappa^F} \right) \frac{a^M}{h_y^2}$ |
| 11 | $-a^M \left(\frac{1}{h_x^2} + \frac{1}{h_y^2} \right) - \left(\frac{\kappa^F}{\kappa^M + \kappa^F} \right) \frac{a^M}{h_y^2}$ | $\frac{a^M}{h_x^2} + \left(1 + \frac{\kappa^F}{\kappa^M + \kappa^F} \right) \frac{a^M}{h_y^2}$ | 0 | $2a^M \left(\frac{1}{h_x^2} + \frac{1}{h_y^2} \right) + \left(\frac{2\kappa^F}{\kappa^M + \kappa^F} \right) \frac{a^M}{h_y^2}$ |
| 12 | $-a^F \left(\frac{2}{h_x^2} + \frac{1}{h_y^2} \right) - \left(\frac{\kappa^M}{\kappa^M + \kappa^F} \right) \frac{a^F}{h_y^2} - \frac{v_0(t)}{h_x}$ | $\frac{2a^F}{h_x^2} + \left(1 + \frac{\kappa^M}{\kappa^M + \kappa^F} \right) \frac{a^F}{h_y^2} + \frac{v_0(t)}{h_x}$ | 0 | $2a^F \left(\frac{2}{h_x^2} + \frac{1}{h_y^2} \right) + \left(\frac{2\kappa^M}{\kappa^M + \kappa^F} \right) \frac{a^F}{h_y^2} + \frac{2v_0(t)}{h_x}$ |
| 13 | $\begin{cases} -a^F \left(\frac{2}{h_x^2} + \frac{1}{h_y^2} \right) - \left(\frac{\kappa^M}{\kappa^M + \kappa^F} \right) \frac{a^F}{h_y^2} - \frac{\bar{v}_0}{h_x}, & A = A^P \\ -a^F \left(\frac{1}{h_x^2} + \frac{1}{h_y^2} \right) - \left(\frac{\kappa^M}{\kappa^M + \kappa^F} \right) \frac{a^F}{h_y^2}, & A = A^N \\ -a^F \left(\frac{1}{h_x^2} + \frac{1}{h_y^2} \right) - \left(\frac{\kappa^M}{\kappa^M + \kappa^F} \right) \frac{a^F}{h_y^2} - \frac{v_0(t)}{h_x} \end{cases}$ | $\begin{cases} a^F + \frac{\bar{v}_0}{h_x}, & A = A^P \\ 0, & A = A^N \end{cases}$ | $\begin{cases} a^F + \frac{\bar{v}_0}{h_x}, & A = A^P \\ 0, & A = A^N \end{cases}$ | $\begin{cases} a^F \left(\frac{3}{h_x^2} + \frac{2}{h_y^2} \right) + \left(\frac{2\kappa^M}{\kappa^M + \kappa^F} \right) \frac{a^F}{h_y^2} + \frac{\bar{v}_0}{h_x}, & A = A^P \\ 2a^F \left(\frac{1}{h_x^2} + \frac{1}{h_y^2} \right) + \left(\frac{2\kappa^M}{\kappa^M + \kappa^F} \right) \frac{a^F}{h_y^2}, & A = A^N \\ 2a^F \left(\frac{1}{h_x^2} + \frac{1}{h_y^2} \right) + \left(\frac{2\kappa^M}{\kappa^M + \kappa^F} \right) \frac{a^F}{h_y^2} + \frac{2v_0(t)}{h_x} \end{cases}$ |
| 14 | $-a^F \left(\frac{1}{h_x^2} + \frac{1}{h_y^2} \right) - \left(\frac{\kappa^M}{\kappa^M + \kappa^F} \right) \frac{a^F}{h_y^2} - \frac{v_0(t)}{h_x}$ | $\frac{a^F}{h_x^2} + \left(1 + \frac{\kappa^M}{\kappa^M + \kappa^F} \right) \frac{a^F}{h_y^2} + \frac{v_0(t)}{h_x}$ | 0 | $2a^F \left(\frac{1}{h_x^2} + \frac{1}{h_y^2} \right) + \left(\frac{2\kappa^M}{\kappa^M + \kappa^F} \right) \frac{a^F}{h_y^2} + \frac{2v_0(t)}{h_x}$ |

Table D.1 Diagonal entries $A_{i_l i_l}$ (centres of Gershgorin circles), radii of Gershgorin circles R_{i_l} , differences J_{i_l} and row sums S_{i_l} of matrices A^P and A^N , $l = 1, \dots, 14$

E Proof of Lemma 4.3

Proof First assertion. Table D.1 shows that the diagonal entries of the matrices A^k , $k = 1, \dots, N_\tau$ are all negative. Thus, we have for all $i = 1, \dots, n$

$$J_i(G^k) = |G_{ii}^k| - \sum_{j=1, j \neq i} |G_{ij}^k| = 1 + \tau\theta(|A_{ii}^k| - \sum_{j=1, j \neq i} |A_{ij}^k|) = 1 + \tau\theta J_i(A^k) \geq 1,$$

since by Lemma D.1 the matrices A^k are diagonal dominant and it holds $J_i(A^k) \geq 0$. Therefore, the matrices $G^k = \mathbb{I}_n - \tau\theta A^k$, $k = 1, \dots, N_\tau$ are strictly diagonal dominant. Lemma C.3 implies that G^k is invertible and $\|(G^k)^{-1}\|_\infty \leq 1/J(G^k) \leq 1$. For $\theta = 0$ it holds $G^k = \mathbb{I}_n$, hence $\|(G^k)^{-1}\|_\infty = \|\mathbb{I}_n\|_\infty = 1$ and the above inequality holds with equality.

Second assertion. We recall the definition of H^k given in (4.2) which reads as $H^k = \mathbb{I}_n + \tau(1 - \theta)A^k$. For $\theta = 1$, we have $H^k = \mathbb{I}_n$, thus for all $\tau > 0$ it holds $\|H^k\|_\infty = 1$ which proves the claim for $\theta = 1$.

Now, let $\theta \in [0, 1]$. We recall that $A^k = A(k\tau)$ takes only the values A^P and A^N . Thus it is sufficient to show that the claim holds for H^P and H^N where $H^{P/N} = \mathbb{I}_n + \tau(1 - \theta)A^{P/N}$. It holds

$$\|H^P\|_\infty = \max_{1 \leq i \leq n} \{S_i(H^P)\}, \text{ with } S_i(H^P) = |1 + \tau(1 - \theta)A_{ii}^P| + \tau(1 - \theta) \sum_{j=1, j \neq i}^n |A_{ij}^P|.$$

Using the fact that all diagonal entries of the matrix A^P are negative, we have for $\tau_i^P = \frac{1}{(1 - \theta)|A_{ii}^P|}$, $i = 1, \dots, n$,

$$|1 + \tau(1 - \theta)A_{ii}^P| = \begin{cases} 1 - \tau(1 - \theta)|A_{ii}^P|, & \text{for } \tau \leq \tau_i^P \\ \tau(1 - \theta)|A_{ii}^P| - 1, & \text{for } \tau > \tau_i^P. \end{cases}$$

This implies that for $i = 1, \dots, n$, we have

$$S_i(H^P) = \begin{cases} 1 - \tau(1 - \theta) \left[|A_{ii}^P| - \sum_{j=1, j \neq i}^n |A_{ij}^P| \right] = 1 - \tau(1 - \theta)R_i(A^P), & \text{for } \tau \leq \tau_i^P, \\ \tau(1 - \theta) \left[|A_{ii}^P| + \sum_{j=1, j \neq i}^n |A_{ij}^P| \right] - 1 = -1 + \tau(1 - \theta)S_i(A^P), & \text{for } \tau > \tau_i^P. \end{cases}$$

Since A^P is weakly diagonal dominant, we distinguish the two cases $J_i(A^P) > 0$ and $J_i(A^P) = 0$. For $J_i(A^P) > 0$, the sum $S_i(H^P)$ is strictly decreasing in τ on $[0, \tau_i^P]$ and strictly increasing in τ on $(\tau_i^P, +\infty)$ and it holds

$$S_i(H^P) \leq 1 \text{ for } \tau \leq \bar{\tau}_i^P := \frac{2}{(1 - \theta)S_i(A^P)} \text{ and } S_i(H^P) > 1 \text{ for } \tau > \bar{\tau}_i^P.$$

For $J_i(A^P) = 0$, we have $S_i(A^P) = 2|A_{ii}^P|$. It holds $S_i(H^P) = 1$ for $\tau \in [0, \bar{\tau}_i^P]$ while $S_i(H^P)$ is strictly increasing in τ on $(\bar{\tau}_i^P, +\infty)$, hence $S_i(H^P) > 1$ for $\tau > \bar{\tau}_i^P$.

Summarizing we obtain

$$\|H^P\|_\infty = \max_{1 \leq i \leq n} S_i(H^P) = 1 \text{ for } \tau \leq \bar{\tau}^P = \min_{1 \leq i \leq n} \bar{\tau}_i^P = \frac{2}{(1 - \theta) \max_{1 \leq i \leq n} S_i(A^P)} = \frac{2}{(1 - \theta)\|A^P\|_\infty},$$

and $\|H^P\|_\infty > 1$ for $\tau > \bar{\tau}^P$. For $A = A^N$ the proof is analogous. Thus, we have

$$\|H^k\|_\infty \leq 1 \text{ for } \tau \leq \min\{\bar{\tau}^P, \bar{\tau}^N\} = \frac{2}{(1 - \theta) \max\{\|A^P\|_\infty, \|A^N\|_\infty\}}.$$

Finally, Lemma D.5 shows that $\max\{\|A^P\|_\infty, \|A^N\|_\infty\} = 4\max\{a^F, a^M\}\left(\frac{1}{h_x^2} + \frac{1}{h_y^2}\right) + \frac{2\bar{v}_0}{h_x} = 2\eta$ which proves the claim.

Third assertion. From the definition of F^k given in (4.2) it follows that for $k = 0, \dots, N_\tau - 1$

$$\begin{aligned}\|F^k\|_\infty &= \|\theta B^{k+1}g^{k+1} + (1-\theta)B^k g^k\|_\infty \leq \theta\|B^{k+1}\|_\infty\|g^{k+1}\|_\infty + (1-\theta)\|B^k\|_\infty\|g^k\|_\infty \\ &\leq (\theta + 1 - \theta)C_B \max_{j=k,k+1}\|g^j\|_\infty \leq C_B \max_{0 \leq j \leq k+1}\|g^j\|_\infty.\end{aligned}$$

where we have used that $B^k = B(k\tau)$ takes only the values B^P and B^N . \square

Acknowledgements The authors thank Thomas Apel (Universität der Bundeswehr München), Martin Bähr, Michael Breuss, Carsten Hartmann, Gerd Wachsmuth (BTU Cottbus–Senftenberg), Andreas Witzig (ZHAW Winterthur), Karsten Hartig (Energie-Concept Chemnitz), Dietmar Deunert, Regina Christ (eZeit Ingenieure Berlin) for valuable discussions that improved this paper.

P.H. Takam gratefully acknowledges the support by the German Academic Exchange Service (DAAD) within the project “PeStO – Perspectives in Stochastic Optimization and Applications”.

R. Wunderlich gratefully acknowledges the support by the Federal Ministry of Education and Research (BMBF) within the project “05M2022 - MONES: Mathematische Methoden für die Optimierung von Nahwärmenetzen und Erdwärmespeichern”.

The work of O. Menoukeu Pamen was supported with funding provided by the Alexander von Humboldt Foundation, under the programme financed by the German Federal Ministry of Education and Research entitled German Research Chair No 01DG15010.

References

1. ARCE, P., MEDRANO, M., GIL, A., ORÓ, E., AND CABEZA, L. F. Overview of thermal energy storage (TES) potential energy savings and climate change mitigation in Spain and Europe. *Applied Energy* 88, 8 (2011), 2764–2774.
2. BAZRI, S., BADRUDDIN, I. A., USMANI, A. Y., KHAN, S. A., KAMANGAR, S., NAGHAVI, M. S., MALLAH, A. R., AND ABDELRAZEK, A. H. Thermal hysteresis analysis of finned-heat-pipe-assisted latent heat thermal energy storage application for solar water heater system. *Case Studies in Thermal Engineering* 40 (2022), 102490.
3. BÄHR, M., BREUSS, M., AND WUNDERLICH, R. Fast explicit diffusion for long-time integration of parabolic problems. In *AIP Conference Proceedings* (2017), vol. 1863, p. 410002, AIP Publishing.
4. BÄHR, M., AND BREUSS, M. *Efficient Long-Term Simulation of the Heat Equation with Application in Geothermal Energy Storage. Mathematics*, (2022), vol. 10, p. 2309.
5. DAHASH, A., OCHS, F., TOSATTO, A., AND STREICHER, W. Toward efficient numerical modeling and analysis of large-scale thermal energy storage for renewable district heating. *Applied Energy* 279 (2020), 115840.
6. DINCER, I., AND ROSEN, M. A. *Thermal energy storage: systems and applications*. John Wiley & Sons, 2021.
7. DUFFY, D. J. *Finite difference methods in financial engineering: a partial differential equation approach*. John Wiley & Sons, 2013.
8. GUELPA, E., AND VERDA, V. Thermal energy storage in district heating and cooling systems: A review. *Applied Energy* 252 (2019), 113474.
9. HAQ, H. M., MARTINKAUPPI, B., HILTUNEN, E., AND SIVULA, T. Simulated thermal response test for ground heat storage: Numerical and analytical modeling of borehole. In *2016 IEEE International Conference on Renewable Energy Research and Applications (ICRERA)* (2016), pp. 291–296.
10. JOHNSON, C. R., AND HORN, R. A. *Matrix analysis*, 2nd ed., Cambridge University Press, 2012.
11. KITAPBAYEV, Y., MORIARTY, J., AND MANCARELLA, P. Stochastic control and real options valuation of thermal storage-enabled demand response from flexible district energy systems. *Applied Energy* 137 (2015), 823 – 831.

12. LI, H., JI, K., TAO, Y., AND TANG, C. Modelling a novel scheme of mining geothermal energy from hot dry rocks. *Applied Sciences* 12, 21 (2022), 11257.
13. MAJOR, M., POULSEN, S. E., AND BALLING, N. A numerical investigation of combined heat storage and extraction in deep geothermal reservoirs. *Geothermal Energy* 6, 1 (2018), 1–16.
14. REGNIER, G., SALINAS, P., JACQUEMYN, C., AND JACKSON, M.D. Numerical simulation of aquifer thermal energy storage using surface-based geologic modelling and dynamic mesh optimisation. *Hydrogeology Journal* 30, (2022), 1179–1198.
15. SANZ-SERNA, J., AND PALENCIA, C. A general equivalence theorem in the theory of discretization methods. *Mathematics of Computation* 45, 171 (1985), 143–152.
16. SOLTANI, M., MORADI KASHKOOLI, F., DEGHANI-SANIJ, A., NOKHOSTEEN, A., AHMADI-JOUGHI, A., GHARALI, K., MAHBAB, S., AND DUSSEAUULT, M. A comprehensive review of geothermal energy evolution and development. *International Journal of Green Energy* 16, 13 (2019), 971–1009.
17. TAKAM, P. H., WUNDERLICH, R., AND PAMEN, O. M. Short-term behavior of a geothermal energy storage: Numerical applications. *arXiv preprint arXiv:2104.05116* (2021).
18. TAKAM, P. H., AND WUNDERLICH, R. On the input-output behavior of a geothermal energy storage: Approximations by model order reduction. *arXiv preprint arXiv:2209.14761* (2022).
19. THOMAS, J. W. *Numerical partial differential equations: finite difference methods*, vol. 22. Springer Science & Business Media, 1995.
20. VARAH, J. M. A lower bound for the smallest singular value of a matrix. *Linear Algebra and its Applications* 11, 1 (1975), 3–5.
21. VARGA, R. S. Geršgorin-type eigenvalue inclusion theorems. In *Geršgorin and His Circles*. Springer, 2004, pp. 35–72.
22. WU, Y., LI, D., YANG, R., MÜSLÜM, A., AND LIU, C. Enhancing heat transfer and energy storage performance of shell-and-tube latent heat thermal energy storage unit with unequal-length fins. *Journal of Thermal Science* (2022), 1–14.
23. ZALBA, B., MARIN, J. M., CABEZA, L. F., AND MEHLING, H. Review on thermal energy storage with phase change: materials, heat transfer analysis and applications. *Applied Thermal Engineering* 23, 3 (2003), 251–283.